Journal of Thermal Analysis and Calorimetry, Vol. 70 (2002) 309–319

INFLUENCE OF NANO-STRUCTURE ON ELECTROLYTIC PROPERTIES IN CeO_2 BASED SYSTEM*

Toshiyuki Mori[1**], *John Drennan*[2], *Yarong Wang*[1], *Ji-Guang Li*[1] *and Takayasu Ikegami*[1]

[1]Advanced Materials Laboratory, National Institute for Materials Science, 1-1 Namiki, Tsukuba, Ibaraki 305-0044, Japan
[2]Centre for Microscopy and Microanalysis, The University of Queensland, St. Lucia, Brisbane, Queensland 4072, Australia

Abstract

Doped ceria (CeO_2) compounds are fluorite type oxides that show oxygen ionic conductivity higher than yttria stabilized zirconia, in oxidizing atmosphere. In order to improve the conductivity, the effective index was suggested to maximize the oxygen ionic conductivity in doped CeO_2 based oxides. In addition, the true microstructure of doped CeO_2 was observed at atomic scale for conclusion of conduction mechanism. Doped CeO_2 had small domains (10–50 nm) with ordered structure in a grain. It is found that the electrolytic properties strongly depended on the nano-structural feature at atomic scale in doped CeO_2 electrolyte.

Keywords: coherent interface, diffuse scattering, doped CeO_2, nano-domain

Introduction

Present status and our strategy for design of doped ceria electrolyte

Doped ceria (CeO_2) systems, which maintain the fluorite structure, have a long history of investigation as potential materials for oxygen ion electrolytes. While the material has found application as oxygen sensors [1, 2], electrochemical cells such as membrane reactors [3, 4], and interlayer structures in certain designs of electrolyte / anode interfaces [5, 6] in fuel cells, the most attractive application of doped CeO_2 would be as the 'solid electrolyte in SOFCs'. The higher ionic conductivity of the material will mean reduced operating temperature, lowering the temperature of operation of the fuel cell means that less expensive materials can be used as interconnects, manifolds and gas transport systems.

---

* This paper was presented at the Second International Symposium on the New Frontiers of Thermal studies of Materials, Yokohama, Japan, November, 2001.

** Author for correspondence: E-mail: MORI.Toshiyuki@nims.go.jp

1418–2874/2002/ $ 5.00

Akadémiai Kiadó, Budapest
Kluwer Academic Publishers, Dordrecht

CeO_2 doped with the oxides of di- or trivalent metals possess higher oxide ionic conductivity than any reported yttria stabilized zirconia electrolytes [7,8]. At high oxygen partial pressures, these CeO_2 based oxides show purely oxide ionic conductivity. At low oxygen partial pressures associated with anodic conditions, however, the Ce^{4+} ion can be partially reduced to Ce^{3+} ion according to the following Eq. (1).

$$O_o^x \rightarrow 1/2O_2 + V_o^{\bullet\bullet} + 2e'(2Ce^{3+}) \quad (1)$$

Quasi-free electrons are introduced into a fluorite lattice in such reducing atmospheres. As a consequence the doped CeO_2 oxides exhibit high oxygen ionic conductivity in oxidizing atmosphere, whereas they are partially reduced and develop electronic conductivity under anodic conditions in the fuel cell. The high ionic conductivity in both oxidizing and reducing atmosphere is an essential requirement for candidate solid electrolyte materials.

Recently, samarium [9, 10] or gadolinium [11, 12] doped CeO_2 electrolytes are attracting much attention from the viewpoint of application in SOFC. It has been considered that these doped CeO_2 electrolytes exhibit high oxygen ionic conductivity due to small association enthalpy between dopant cation and oxygen vacancy in fluorite lattice [13]. On the other hand, La doped CeO_2 has a comparable association enthalpy with that of the gadolinium doped CeO_2 electrolyte [14]. Accordingly, it is concluded that Sm or La doped CeO_2 is one of promising solid electrolytes in SOFC for low or intermediate temperature operation.

The authors suggested a strategy to improve the oxide ionic conductivity in both oxidizing and reducing atmosphere [15]. Using simple crystallographic principles we suggested an approach to electrolyte design that maximized the usefulness of electrolyte materials. In the present study, the authors re-introduce the concept of effective index and examine the relationship between true microstructures of prepared specimens and electrolytic properties to conclude the conduction mechanism of doped CeO_2 electrolytes.

Definition of effective index

In general, simplest model for the ionic conduction in a grain is given by the random-walk theory [16],

$$\sigma_{ion} = NcCq\mu_0 = (A/T)\exp(-E_a/kT) \quad (2)$$

$$A = f(z/6)(Cq^2/k)N_c(1-N_c)l^2\nu_0\exp(\Delta S_m/k) \quad (3)$$

where oxygen ion mobility $\mu_0 = qD/kT$ is given by the Einstein equation for diffusive motion of a carrier of charge q, the diffusion coefficient $D=D_0\exp(-\Delta G_m/kT)$ contains the motional free energy $\Delta G_m=\Delta H_m-T\Delta S_m$ for a jump to a vacant or equivalent near neighbor site, l is a jump distance to the number of nearest neighbor sites (z), ν_0 is an optical mode attempt frequency (10^{12}–10^{13} Hz) for a ion jump, N_c is the fraction of occupied sites, C corresponds to the density of ion sites in the sub lattice, and f is geometrical factor depending on a jump path. In the case of the fluorite structure, l=a/2,

(a: lattice constant), z=6, f=1, C=4a^{-3}, q=2e, (e: electron charge). The ionic conductivity in fluorite becomes

$$\sigma_{ion} = (4e^2/akT)N_c(1-N_c)\nu_0 \exp(\Delta S_m/k)\exp(-E/kT) \quad (4)$$

Activation energy (E) *in* fluorite is expressed as Eq. (5) [16]

$$E = E_m + (n/2)E_a \quad (5)$$

where E_m is migration energy and E_a means association energy between vacancy and dopant cation, n equals 1 or 2 for di- or trivalent dopants, respectively. In a classical perfect crystal, all normal sites are fully occupied (N_c=1) or all interstitial sites are empty (N_c=0). This is expected to lead to highly insulating characteristics. In high quality electrolyte with defect structure, N_c must approach 1/2. This corresponds to nearly all of the ions on a given sub lattice being mobile. Moreover, the crystal structure should be such that easy motion of oxygen ions from one equivalent site to the neighbor equivalent site is possible. This is reflected in exceptionally low value for E. In other words, the suggested approach for fast oxygen ionic conduction should simultaneously satisfy two criteria which are, indication of condition for $N_c \approx 1/2$ and clarification of the ideal crystallographic configuration in the fluorite lattice.

The effective index for fast oxygen ionic conduction in doped CeO_2 electrolytes was defined using ionic radii and the amount of oxygen vacancies that are produced by the dopant substituting on idealized crystallographic sites. According to Pauling's first rule, the crystallographic coordination number of a cation is decided by the radius ratio between cation and anion. The coordination number of the cation, in the case of oxides, dominates the crystal structure. The crystal structure of CeO_2 based oxide is the fluorite type lattice. The coordination number of the cation in the idealized fluorite type structure is eight. For stable formation of the fluorite structure, the ionic radius between the cation (r_c) and anion (r_a) ranges from 0.732 to 1 in the case of eight fold coordination. Up until now this ratio (r_c/r_a) was not considered as a controlling factor in the ionic conductivity because it seemed to have no direct relationship to the defect structure of fluorite. However, this ratio can be effectively utilized by controlling it in conjunction with the oxygen vacancy levels. On the other hand, Kilner *et al*. indicated that association enthalpy between dopant cation and oxygen vacancy was minimized when the ionic radius mismatch between dopant cation and host element is least [17]. Accordingly, it is inferred that the oxygen ionic conductivity in fluorite could be enhanced by decrease of this ionic radius mismatch. However, ionic radius ratio lacked of the viewpoint of crystallography.

In the present study, the effective index was defined to Eq. [6] as an original index instead of the (r_c/r_a) or (r_d/r_h).

$$\text{Effective index} = (\text{avg}.r_c/\text{eff}.r_o)(r_d/r_h) \quad (6)$$

where δ is the average ionic radius of cation, and eff.r_o is the effective oxygen ionic radius, which can be given by

$$\text{eff}.r_o = 1.4\{(2-\delta)/2\} \quad (7)$$

where δ is the level of oxygen vacancies in the doped CeO_2 based oxide, and 1.4 is the commonly used ionic radius (Å) of oxygen in oxides. The term r_d refers to the average ionic radius of dopant, and r_h is the ionic radius of host element (Ce^{4+}).

The first term (avg.r_c/eff.r_o) in Eq. (6) becomes 1 when the cation is coordinated by eight anions in a non-distorted fluorite crystal structure. The second term (r_d/r_h) in Eq. (6) approaches 1 when the association enthalpy between dopant cation and anion vacancy is minimized in the case of fluorite structure. Therefore, it is assumed that the doped CeO_2 electrolytes reach the ideal fluorite structure for high oxygen ionic conduction when the effective index goes toward one. The authors conclude that the first and second terms in Eq. (6) correspond to clarification of an ideal configuration in fluorite and an indication of the condition for $N_c \approx 1/2$ in the fluorite lattice, respectively.

In order to confirm the validity of the suggested index, various kinds of Sm- or La-doped CeO_2 based oxides were prepared by co-precipitation method, and characterized as the specimen with low, intermediate, or high index, respectively. The microstructure of the sintered body was investigated to conclude the conduction mechanism using TEM. The electrolytic properties (electrical conductivity, P_{O_2} dependence of conductivity, and operation properties) of doped CeO_2 based materials were also evaluated.

Experimental

Preparation of powder and sintered body

The starting materials were commercial $Ce(NO_3)_3 \cdot 6H_2O$ powder (purity: 99.9%; Wako Chemicals Co. Ltd., Japan), $Sm(NO_3)_3 \cdot 6H_2O$ powder (purity: 99.95%, Kanto Chemical Co. Inc., Japan), $Ca(NO_3)_2$ and $Ba(NO_3)_2$ powders (purity: 99.95%, Kanto Chemical Co. Inc., Japan). Each powder was dissolved in distilled water and mixed in order to prepare the composition of $Sm_xCe_{1-x}O_{2-\delta}$ (x=0.2 and 0.25), $La_xCa_xCe_{1-x}O_{2-\delta}$ (x=0.125, 0.15 and 0.175), $(Sm_{0.5}Ca_{0.5})_xCe_{1-x}O_{2-\delta}$ (x=0.175, 0.20, 0.225 and 0.25), $(La_{1-x}Sr_{0.2}Ba_x)_{0.175}Ce_{0.825}O_{2-d}$ (x=0.03 and 0.05). NH_3+$(NH_4)_2CO_3$ solution [$NH_3/(NH_4)_2CO_3$=1/1] was dropped into the mixed solution for precipitation. In order to provide $(Sm_{0.936}Cs_{0.06}Li_{0.004})_xCe_{1-x}O_{2-\delta}$ (x= 0.20, 0.225, 0.250 and 0.275), Li_2O powder (purity: 99.9%; Kishida Chemicals Co. Ltd., Japan) and Cs_2CO_3 powder (purity: 99.9%; Wako Chemicals Co. Ltd., Japan) were added to the prepared Sm_2O_3–CeO_2 mixture in the specified composition using the co-precipitation method. These powder mixtures were mixed, dried, and calcined at 1000°C for 1 h. Sintering was performed at 1450–1550°C for 4 h.

Sample characterization

Elements in the powders were measured using the following methods: Ce, La, Sm, Sr and Ba were measured using the inductively coupled plasma (ICP) technique, and Cs and Li were measured using glow discharge mass spectroscopy (GDMS).

For detailed examination of influence of nanostructure on electrolytic properties, four representative specimens were selected. The crystal phase was identified using X-ray diffraction analysis and selected area electron diffraction analysis. An electron diffraction pattern was calculated using the software CaRlne Crystallography version 3.1 (presented by Boudias and Monceau). The microstructures of these four representative specimens were analyzed using TEM. TEM observation was performed with gun voltages of 200 keV (JEOL 2010) and 400 KeV (JEOL 4010).

Measurement of electrical properties

Electrical conductivity of the sintered specimens was measured by dc-four point measurements at 800°C and dc-three point measurements at 400–800°C. The dimensions of the specimens were 10 mm in a diameter and 2 mm in thickness for three point measurements and 10×2 mm and 30 mm in length for four point measurements. The oxygen partial pressure (P_{O_2}) dependence of conductivity was measured at 800°C. The P_{O_2} was controlled using zirconia pump from 10^{-3} to 10^{-17} atm and it was checked by zirconia oxygen sensor. The relaxation time of before measurement was approximately four hours. The operation properties of the fuel cell were measured by the following oxygen-hydrogen cell.

$$O_2\,1\,\text{atm},C\,\big|\,\text{doped}\,CeO_2\,\big|\,A,\quad H_2-H_2O\,(40℃)\,1\,\text{atm}$$

where cathode *C*=$La_{0.9}Sr_{0.1}MnO_3$ and anode *A*=Ni/YSZ cermet (Ni:YSZ = 55:45 in volume ratio). The dimensions of the electrolyte were 30×30 mm and 0.5 mm thickness. The discharge performance of the cell was investigated at 700, 800, 900, and 1000°C.

Results and discussion

Figure 1 shows the relationship between the effective index and the electrical conductivity of 15 specimens at 800°C in air. The specimens in Fig. 1 do not have open pore in the specimens. The relative densities of them were over 95%. As this figure indicates, the electrical conductivity increased with an increase of suggested index, confirming the utility of suggested index. Since the ionic transport number of all specimens remains unity at 800°C, the enhancement of electrical conductivity in Fig. 1 is attributable to an increase of oxygen ionic conductivity in doped CeO_2 electrolytes. Table 1 summarizes the chemical composition in five representative specimens. The chemical analysis showed that the specimen composition was controlled well with only a very small deviation. It is concluded that the suggested index of all specimens can be calculated using the starting composition of the specimens. In addition, the apparent activation energy of $Sm_{0.2}Ce_{0.8}O_{1.90}$, $(Sm_{0.5}Ca_{0.5})_{0.225}Ce_{0.775}O_{1.84}$, $(Sm_{0.936}Cs_{0.06}Li_{0.004})_{0.25}Ce_{0.75}O_{1.86}$, and $(La_{0.75}Sr_{0.2}Ba_{0.05})_{0.175}Ce_{0.825}O_{1.891}$ was 88.0, 72.4, 68.1, and 67.3 kJ mol^{-1}, respectively. These results give us message that the composition and microstructure guided by suggested index would play a key role for improvement of oxygen ionic conductivity.

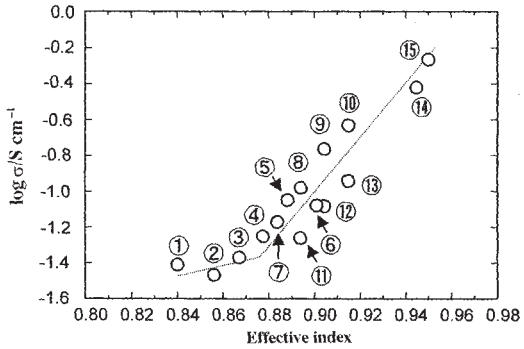

Fig. 1 Relationship between effective index and electrical conductivity. Measurement temperature: 800°C, measurement atmosphere: air,
1 – $Sm_{0.2}Ce_{0.8}O_{1.90}$, 2 – $Sm_{0.25}Ce_{0.75}O_{1.875}$, 3 – $(Sm_{0.5}Ca_{0.5})_{0.175}Ce_{0.825}O_{1.87}$,
4 – $(Sm_{0.5}Ca_{0.5})_{0.20}Ce_{0.80}O_{1.85}$, 5 – $(Sm_{0.5}Ca_{0.5})_{0.225}Ce_{0.775}O_{1.84}$,
6 – $(Sm_{0.5}Ca_{0.5})_{0.25}Ce_{0.75}O_{1.81}$, 7 – $(Sm_{0.936}Cs_{0.06}Li_{0.004})_{0.2}Ce_{0.8}O_{1.89}$,
8 – $(Sm_{0.936}Cs_{0.06}Li_{0.004})_{0.225}Ce_{0.775}O_{1.88}$, 9 – $(Sm_{0.936}Cs_{0.06}Li_{0.004})_{0.25}Ce_{0.75}O_{1.87}$,
10 – $(Sm_{0.936}Cs_{0.06}Li_{0.004})_{0.275}Ce_{0.725}O_{1.85}$, 11 – $La_{0.125}Ce_{0.875}O_{1.94}$,
12 – $La_{0.15}Ce_{0.85}O_{1.925}$, 13 – $La_{0.175}Ce_{0.825}O_{1.91}$,
14 – $(La_{0.77}Sr_{0.2}Ba_{0.03})_{0.15}Ce_{0.85}O_{1.892}$, 15 – $(La_{0.75}Sr_{0.2}Ba_{0.05})_{0.175}Ce_{0.825}O_{1.891}$

Figure 2 shows one example of oxygen-partial-pressure dependence of the conductivity at 800°C. The P_{O_2} dependence of the conductivity consists of two regions. One is the ionic conductive region and the other is *n*–type semi-conductive region. In the ionic conductive region, the conductivity is constant against P_{O_2}. The conductivity increases in the *n*-type region with decreasing P_{O_2}. The relationship between the logarithm of conductivity and the logarithm of P_{O_2} has a slope of 1/4 [18]. The *n*-type conduction appears because the number of conductive electrons is increased by a reduction of CeO_2. The ionic conductivity of $Sm_{0.2}Ce_{0.8}O_{1.9}$ with low index is constant up to around $P_{O_2}=10^{-8}$ atm, but the conductivity increased with de-

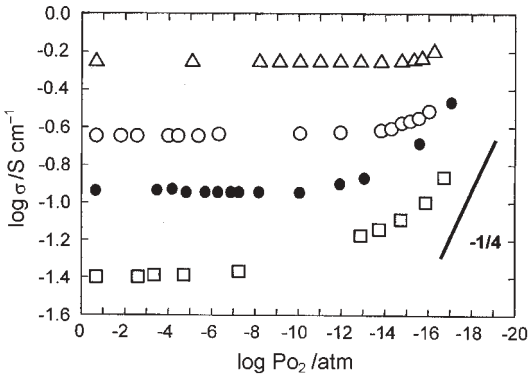

Fig. 2 Oxygen-partial-pressure dependence of conductivity at 800°C; □ – $Sm_{0.2}Ce_{0.8}O_{1.90}$, ● – $(Sm_{0.936}Cs_{0.06}Li_{0.004})_{0.25}Ce_{0.75}O_{1.87}$, ○ – $La_{0.175}Ce_{0.825}O_{1.91}$, △ – $(La_{0.75}Sr_{0.2}Ba_{0.03})_{0.175}Ce_{0.825}O_{1.891}$

creasing P_{O_2} below $P_{O_2}=10^{-8}$ atm, due to the reduction of this specimen. On the other hand, the ionic conductive region of $(La_{0.75}Sr_{0.2}Ba_{0.05})_{0.175}Ce_{0.825}O_{1.891}$ with high index continued up to a lower P_{O_2} region than that of $Sm_{0.2}Ce_{0.8}O_{1.9}$. Accordingly, it is concluded that the ionic domain of doped CeO_2 based material with high suggested index was apparently expanded by the enhancement of ionic conductivity. Moreover, this tendency indicates that suggested index would be a useful tool for design of solid electrolyte.

Table 1 Chemical composition of specimens

Sample	Chemical composition
$Sm_{0.25}Ce_{0.75}O_{1.88}$	$Sm_{0.242}Ce_{0.758}O_{1.88}$
$(Sm_{0.5}Ca_{0.5})_{0.225}Ce_{0.775}O_{1.84}$	$(Sm_{0.496}Ca_{0.468})_{0.225}Ce_{0.783}O_{1.84}$
$(Sm_{0.936}Cs_{0.06}Li_{0.004})_{0.25}Ce_{0.75}O_{1.86}$	$(Sm_{0.936}Cs_{0.06}Li_{0.004})_{0.250}Ce_{0.746}O_{1.86}$
$La_{0.175}Ce_{0.825}O_{1.91}$	$La_{0.178}Ce_{0.822}O_{1.91}$
$(La_{0.175}Sr_{0.2}Ba_{0.05})_{0.175}Ce_{0.825}O_{1.891}$	$(La_{0.751}Sr_{0.198}Ba_{0.051})_{0.175}Ce_{0.823}O_{1.890}$

Figure 3 displays the XRD patterns of four representative specimens, $Sm_{0.2}Ce_{0.8}O_{1.9}$, $(Sm_{0.936}Cs_{0.06}Li_{0.004})_{0.25}Ce_{0.75}O_{1.86}$, $La_{0.175}Ce_{0.825}O_{1.91}$, and $(La_{0.75}Sr_{0.2}Ba_{0.05})_{0.175}Ce_{0.825}O_{1.891}$. As this figure indicates, these specimens consisted of fluorite structure. No other phases

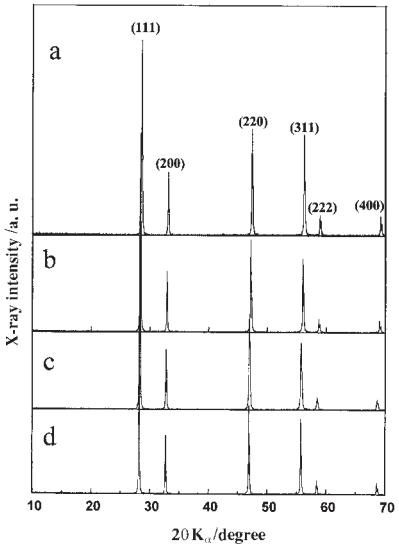

Fig. 3 X-ray diffraction patterns of a – $Sm_{0.2}Ce_{0.8}O_{1.9}$, b – $(Sm_{0.936}Cs_{0.06}Li_{0.004})_{0.25}Ce_{0.75}O_{1.86}$, c – $La_{0.175}Ce_{0.825}O_{1.912}$, and d – $(La_{0.75}Sr_{0.2}Ba_{0.05})_{0.175}Ce_{0.825}O_{1.891}$

seemed to be observed in XRD patterns. And the other specimens in Fig. 1 had same flu-

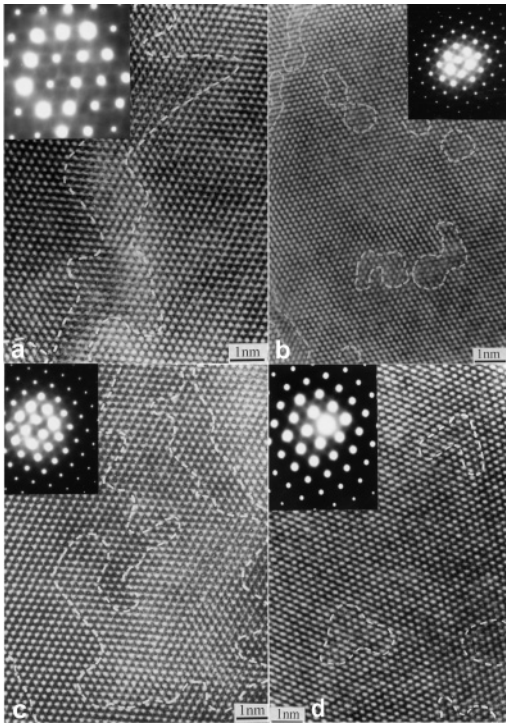

Fig. 4 Selected area electron diffraction patterns (<110>$_F$) and high resolution lattice images (<110>$_F$) recorded from sintered bodies of a – $Sm_{0.2}Ce_{0.8}O_{1.9}$, b – $(Sm_{0.936}Cs_{0.06}Li_{0.004})_{0.25}Ce_{0.75}O_{1.86}$, c – $La_{0.175}Ce_{0.825}O_{1.912}$, and d – $(La_{0.75}Sr_{0.2}Ba_{0.05})_{0.175}Ce_{0.825}O_{1.891}$, dashed line area means domain with ordered structure

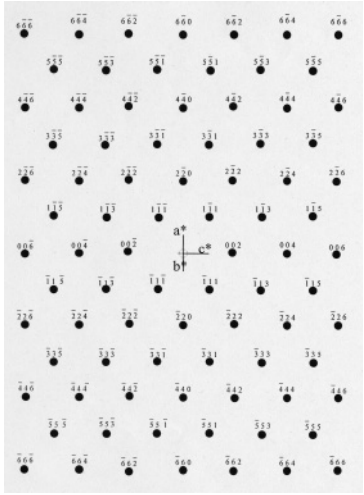

Fig. 4e Calculated electron diffraction pattern of $[110]_F$ zone

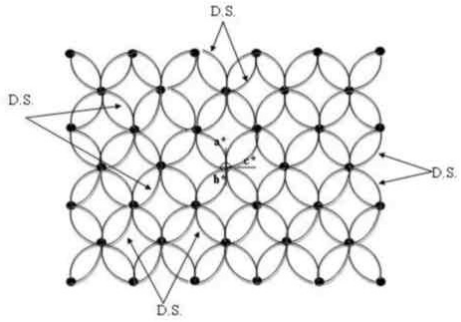

Fig. 4f The illustrated image of diffuse scattering in the background of electron diffraction pattern $[110]_F$ zone, where D.S. means diffuse scattering

orite pattern. In order to conclude the mechanism of enhancement of conductivity, selected area electron diffraction pattern and microstructure of aforementioned four specimens were observed by TEM.

Figures 4a–d display the lattice images and electron diffraction patterns in grain of aforementioned four specimens. For comprehension of diffraction pattern, calculated diffraction pattern was illustrated in Fig. 4e. The diffuse scattering, as illustrated in Fig. 4f, clearly appeared in the background of all electron diffraction patterns. On the other hand, extra spots cannot be observed in the electron diffraction patterns. This diffuse scattering indicates that these specimens have very small domains with short range ordered structure and the interface between the domain and fluorite lattice is coherent in a grain [19]. If the interface has a misfit, the extra spots will be appeared in the diffraction patterns. Moreover, high-resolution images indicate that dashed line area is a domain and the domain has irregular shape. While $Sm_{0.2}Ce_{0.8}O_{1.9}$ sintered body with low index value has big domain in a grain, $(La_{0.75}Sr_{0.2}Ba_{0.05})_{0.175}Ce_{0.825}O_{1.89}$ and $(Sm_{0.936}Cs_{0.06}Li_{0.004})_{0.25}Ce_{0.75}O_{1.86}$ sintered bodies with high index values has very small nano sized domain (i.e. around 10 nm) in a grain. The authors conclude that a large strain in the lattice of doped CeO_2 would

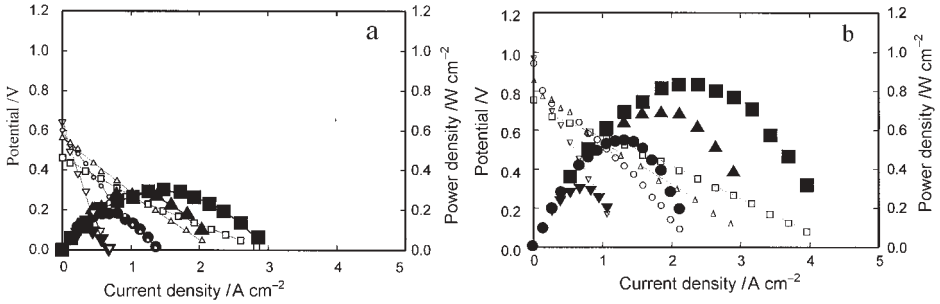

Fig. 5 Discharge performance of a – $Sm_{0.2}Ce_{0.8}O_{1.9}$ and b – $(La_{0.75}Sr_{0.2}Ba_{0.05})_{0.175}Ce_{0.825}O_{1.891}$. Small open symbols indicate the potential as a function of current density: □ – 1000, △ – 900, o – 800, ▽ – 700°C. Large closed symbols indicate the power density as a function of current density: ■ – 1000, ▲ – 900, ● – 800, ▼ – 700°C. Electrolyte thickness: 0.5 mm

be created by doping lower valance cation in Ce site. In order to minimize the strain in the lattice, domain would be prepared in the lattice. Therefore, it is concluded that domain size is minimized in non-distorted fluorite structure. On the other hand, suggested index indicates research direction to prepare a non-distorted fluorite structure as a high quality electrolyte. Accordingly, the specimen with high index value would have nano-sized domain and show high conductivity.

Figures 5a and 5b demonstrate operation properties of $Sm_{0.2}Ce_{0.8}O_{1.9}$ with low index value and $(La_{0.75}Sr_{0.2}Ba_{0.05})_{0.175}Ce_{0.825}O_{1.89}$ with high index value. Terminal potential and maximum power density of $(La_{0.75}Sr_{0.2}Ba_{0.05})_{0.175}Ce_{0.825}O_{1.89}$ with high index value was much higher than those of $Sm_{0.2}Ce_{0.8}O_{1.9}$ with low index due to enhancement of oxygen ionic conductivity.

Conclusions

The effective index, as criterion for fast oxide ionic conduction in doped CeO_2, was suggested using ionic radii and expected oxygen vacancy level in order to improve electrolytic properties. The relationship between nano-structure and electrolytic properties was examined. The results obtained are summarized as follows;

- The electrolytic properties such as ionic conductivity, apparent activation energy, P_{O_2} dependence of conductivity, and power density of the specimens increased with increasing suggested index. Therefore, the authors expect that superior quality solid electrolyte will be created using the concept of suggested index.
- The author observed nano–size domain with ordered structure in doped CeO_2 sintered body. The size of domain in the microstructure of the specimens with high index value was very small as compared with that in the previous reported doped CeO_2 electrolyte such as $Sm_{0.2}Ce_{0.8}O_{1.9}$ sintered body. The electrolytic properties seem to strongly depend on the nano-featured structure at atom level in doped CeO_2 electrolytes. It is concluded that the control of size and distribution of nano-domain are important for design of superior quality doped CeO_2 electrolytes in future.

In addition, the authors would like to point out that a combination approach between electrical measurement and nano-structure characterization is required to develop solid electrolytes.

References

1 J. Fouletier and M. Henault, Solid State Ionics, 9–10 (1983) 1277.
2 T. Inoue, N. Seki, K. Eguchi and H. Arai, J. Electrochem. Soc., 137 (1990) 2523.
3 S. Hamakawa, T. Hayakawa, A. P. E. York, T. Tsunoda, Y. S. Yoon, K. Suzuki, M. Shimizu and K. Takehira, J. Electrochem. Soc., 143 (1996) 1264.
4 S. Hamakawa, T. Hayakawa, T. Tsunoda, K. Suzuki, K. Murata and K. Takehira, Electrochemical Solid State Lett., 1 (1998) 220.
5 T. Tsai and S. A. Barnett, J. Electrochem. Soc., 145 (1998) 1696.
6 E. P. Murray, T. Tsai and S. A. P. Barnett, Nature, 400 (1999) 649.

7 D. Singman, J. Electrochem. Soc., 113 (1966) 502.
8 D. L. Maricle, T. E. Swarr and S. Karavolis, Solid State Ionics, 52 (1992) 173.
9 M. Gödickemeier and L. J. Gauckler, J. Electrochem. Soc., 145 (1998) 414.
10 C. Milliken, S. Guruswamy and A. Khandkar, J. Electrochem. Soc., 146 (1999) 872.
11 T. Kudo and H. Obayashi, J. Electrochem. Soc., 123 (1976) 415.
12 R. Doshi, V. L. Richards, J. D. Carter, X. Wang and M. Krumpelt, J. Electrochem. Soc., 146 (1999) 1273.
13 J. A. Kilner and C. D. Waters, Solid State Ionics, 6 (1982) 253.
14 V. Butler, C. R. A. Catlow, B. E. F. Fender and J. H. Harding, Sold State Ionics, 8 (1983) 109.
15 T. Mori, T. Ikegami, H. Yamamura and T. Atake, J. Therm. Anal. Cal., 57 (1999) 831.
16 J. A. Kilner and R. J. Brook, Solid State Ionics, 6 (1982) 237.
17 J. A. Kilner, Solid State Ionics, 129 (2000) 13.
18 Y. M. Chiang, D. Birnie III and W. D. Kingery, in Physical Ceramics, Principles for Ceramic Science and Engineering, John Wiley & Sons, Inc., New York 1996, p. 136.
19 D. B. Williams and C. B. Carter, Transmission Electron Microscopy, Diffraction II, Plenum Publishing Corporation, New York 1996, p. 259.